

# Recent studies on thermophysical properties of metallic alloys with PROSPECT: Excess properties to construct a solution model

H. FUKUYAMA\*, M. WATANABE AND M. ADACHI

*Institute of Multidisciplinary Research for Advanced Materials, Tohoku University,  
2-1-1 Katahira, Aoba-ku, Sendai, 980-8577, Japan*

*Received: July 31, 2019; Accepted: November 13, 2019.*

We have developed the system PROSPECT for measuring thermophysical properties at high temperature. Precise thermophysical measurements provide accurate excess functions, which represent non-ideality of solutions. We use excess functions to discuss solution models on the basis of electronic structure and thermodynamics. Pd-Fe systems show positive excess volume  $V^E$  with negative excess Gibbs energy  $G^E$ . The phase diagrams of these systems have common features with those of other Pd-X and Pt-X systems (where X is Fe, Ni, Co, or Cu), which means they all have order-disorder transitions. The correlation between  $V^E$  and  $G^E$  is discussed in terms of the electronic structure of the alloys, and an energy diagram is proposed to understand this correlation. The excess heat capacity  $C_p^E$  of Fe-Ni melts is positive over a whole composition range and a wide temperature range. We estimate the temperature dependences of the excess enthalpy  $H^E$  and excess entropy  $S^E$  of Fe-Ni melts from  $C_p^E$ . The Lupis-Elliott rule is satisfied for  $H^E$  and  $S^E$  with positive  $C_p^E$ .

*Keywords:* Thermophysical properties, electromagnetic levitation, density, excess volume, heat capacity, excess heat capacity, modulation calorimetry, binary alloys, liquid metals

## 1 INTRODUCTION

Additive manufacturing has rapidly transformed material manufacturing technologies. Material informatics, which combines data and material

---

\*Corresponding author: hiroyuki.fukuyama.b6@tohoku.ac.jp

science, is rising and helping not only to explore new materials but also to reduce the development time of materials. First-principle calculation is mostly used for studying nano-scale crystal structure and exploring new materials. For macro-scale material processes, numerical simulation of heat and mass transfer is a powerful optimization tool that needs to be further developed. Accuracy of simulation highly depends on the database of thermophysical properties of materials; therefore, improving the database is critical especially for unknown conditions such as ultrahigh temperature and pressure for highly reactive materials. Here, we show that although data-driven material design is important, an experimental database is still highly valuable as a source of primary data.

We developed the system PROSPECT in 2009 for measuring thermophysical properties at high temperature. PROSPECT features electromagnetic levitation with a static magnetic field, which enables highly accurate measurements of density, surface tension, normal spectral emissivity, hemispherical total emissivity, heat capacity, and thermal conductivity of metallic melts [1–21]. Figure 1 shows the schematic of PROSPECT, which consists of an electromagnetic levitator, a superconducting magnet, a laser, a high-speed camera, vacuum pumps, a gas supply, a radiation pyrometer, and an rf-electric source, which are operated on a LabVIEW-based platform.

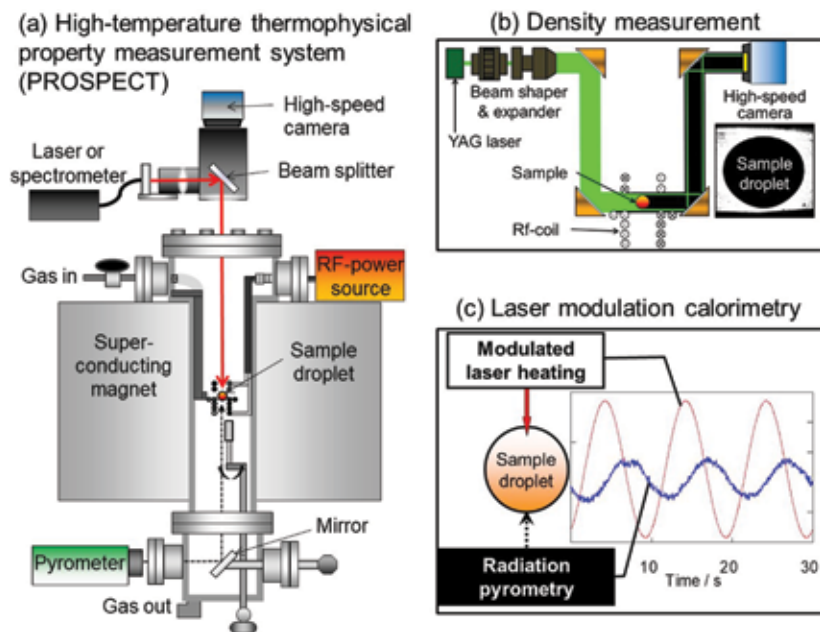


FIGURE 1

(a) Schematic of high-temperature thermophysical property measurement system PROSPECT, (b) auxiliary setup for density measurement, and (c) modulation laser calorimetry.

Materials we have studied with PROSPECT are:

- single elements such as Pt [1], Si [2,3], Fe [4–8], Ni [6], Cu [9,10], Co [11], Ti [12], Pd, and Au
- binary alloys such as Fe-(Ni [13,14], Cu), Ni-Al [15], Pd-(Fe, Ni, Cu) [16], Si-(Fe, Ni, Ge) [17], and Cu-Co [18], Ti-(Cu, Ni) [19], Pt-(Fe, Co, Ni, Cu) [20], Au-(Cu, Pd, Ni)
- industrial alloys such as stainless steels types 304, 316, and 420, Inconel 718, Ti-6Al-4V, Co-Cr-Mo, and Mo-Si-B-Ti-C
- nuclear power plant materials such as the stainless steel-B<sub>4</sub>C mixture [21]

The obtained thermophysical properties have been used to simulate various processes such as crystal growth, refining, casting, welding, and additive manufacturing. The data for the stainless steel-B<sub>4</sub>C mixture are required for modeling severe accidents in nuclear power plants.

Highly accurate thermophysical data obtained with PROSPECT not only satisfy industrial demands, but help develop a solution theory. A thermodynamic excess property represents the deviation of a real solution from ideality. Precise measurements provide accurate excess properties with which to model real solutions. In this paper, we study the excess molar volume and heat capacity measured for binary solutions. We use these excess functions to discuss a solution model on the basis of electronic structure and thermodynamics.

## 2 EXCESS FUNCTIONS

A thermodynamic excess function  $X^E$  of a real solution is defined by the difference between the observed thermodynamic mixing function  $\Delta_{\text{mix}}X$  and the function for an ideal solution,  $\Delta_{\text{mix}}X^{\text{ideal}}$ :

$$X^E = \Delta_{\text{mix}}X - \Delta_{\text{mix}}X^{\text{ideal}}. \quad (1)$$

The corresponding excess functions are:

(a) excess volume

$$V^E = \Delta_{\text{mix}}V - \Delta_{\text{mix}}V^{\text{ideal}} = \Delta_{\text{mix}}V, \quad (2)$$

(b) excess enthalpy

$$H^E = \Delta_{\text{mix}}H - \Delta_{\text{mix}}H^{\text{ideal}} = \Delta_{\text{mix}}H, \quad (3)$$

(c) excess entropy

$$S^E = \Delta_{\text{mix}}S - \Delta_{\text{mix}}S^{\text{ideal}} = \Delta_{\text{mix}}S + R \sum_{i=1}^n (x_i \ln x_i), \quad (4)$$

(d) excess Gibbs energy

$$\begin{aligned} G^E &= \Delta_{\text{mix}}G - \Delta_{\text{mix}}G^{\text{ideal}} = (\Delta_{\text{mix}}H - T\Delta_{\text{mix}}S) + T\Delta_{\text{mix}}S^{\text{ideal}}, \\ &= (\Delta_{\text{mix}}H - T\Delta_{\text{mix}}S) - RT \sum_{i=1}^n (x_i \ln x_i) \end{aligned} \quad (5)$$

(e) excess heat capacity at constant pressure

$$C_P^E = \Delta_{\text{mix}}C_P - \Delta_{\text{mix}}C_P^{\text{ideal}} = \Delta_{\text{mix}}C_P. \quad (6)$$

Here, all functions are molar values. The excess volume, enthalpy, and heat capacity are equal to the volume, enthalpy, and heat capacity of mixing for a real solution, respectively, because the ideal mixing values are zero in each case. The ideal mixing volume  $\Delta_{\text{mix}}V^{\text{ideal}}$  is zero because the volume is given by  $V = \left( \frac{\partial G}{\partial p} \right)_T$  from the fundamental relation of chemical thermodynamics where  $\Delta_{\text{mix}}G^{\text{ideal}} (= RT \sum_{i=1}^n (x_i \ln x_i))$  is independent of pressure. The ideal mixing heat capacity  $\Delta_{\text{mix}}C_P^{\text{ideal}}$  is also zero because the heat capacity is given by  $C_P = \left( \frac{\partial H}{\partial T} \right)_p$ , where  $\Delta_{\text{mix}}H^{\text{ideal}}$  is always zero (i.e., independent of temperature).

### 3 EXCESS VOLUME

#### 3.1 Density measurement

The density of a liquid metal is a fundamental and important property not only for evaluating buoyancy convection in simulations but also for determining thermal conductivity and surface tension. PROSPECT uses electromagnetic levitation in a static magnetic field as shown in Fig. 1. Oscillation of a sample droplet causes a large uncertainty in the density measurement using conventional levitation techniques, which evaluate droplet volume by recording droplet images horizontally. PROSPECT provides static levitation by applying a static magnetic field, which effectively suppresses oscillation and translational motion of a sample droplet, enabling highly accurate density measurement without contact [13].

Figure 1(b) shows the schematic of the experimental setup for measuring density. The spatial distribution of the laser beam intensity (with a wavelength of 532 nm) is homogenized, and its radius is expanded to cover the sample droplet. The laser beam irradiates the droplet, and its shadow is recorded by a high-speed camera. The edge of the droplet is extracted from the droplet images, and the shape of the edge is numerically approximated

with a Legendre polynomial. Assuming axial symmetry of the droplet image, the droplet volume is determined by integrating the polynomial equation. Here, we use the average between the sample mass before and after the experiment to determine the density.

### 3.2 Density and excess volume of Pd-Fe melts

Figure 2 shows the temperature dependence of the density of the Pd-Fe binary melts for each alloy composition [16]. The density linearly decreases with increasing temperature for each alloy. The abbreviation M.P. in the figure is melting temperature, and L.T. is liquidus temperature. Thus, we succeeded in measuring the density of the alloy melts including their deep undercooling regions.

Figure 3(a) shows the variation of the molar volume of the Pd-Fe melts with composition at 1873 K. The error bars indicate the expanded uncertainty. The obtained molar volume positively deviates from that of an ideal solution represented by the black dashed line. The difference between molar volumes of real and ideal solutions is the excess volume ( $V^E$ ). Figure 3(b) shows the variation of the excess volume of the melts with composition at 1873 K and 1760 K. The excess volume is small at both ends of the alloy composition range but reaches almost 10% of the molar volume for a concentrated alloy. This shows that deviations from ideality may be significant

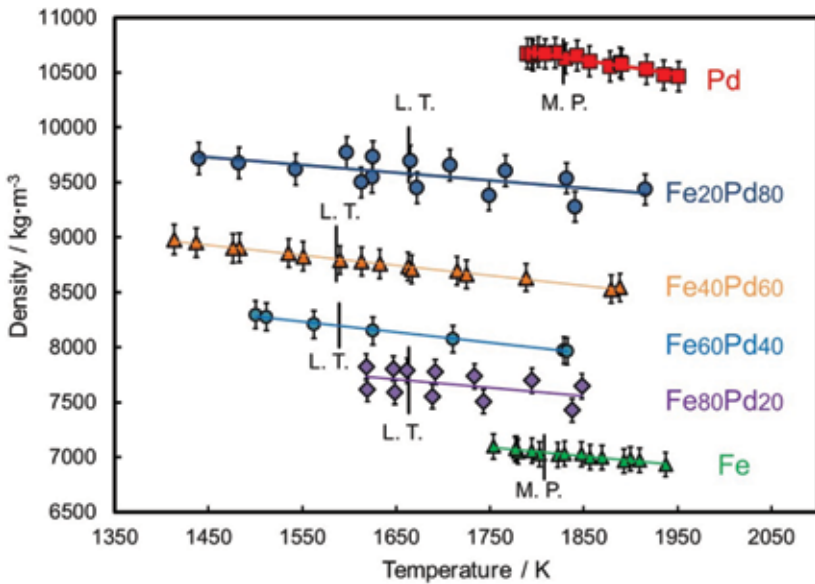


FIGURE 2  
Temperature dependence of the density of Pd-Fe binary melts for each alloy composition [16]. M.P. is the melting point of Fe or Pd. L.T. is the liquidus temperature for each alloy.

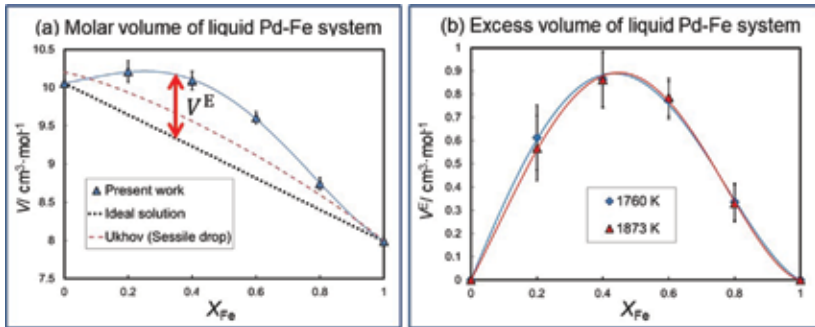


FIGURE 3

(a) Variation of the molar volume of Pd-Fe melts with composition at 1873 K, and (b) variation of the excess volume of the melts with composition at 1873 K and 1760 K [16]. Ukhov and colleagues [22] obtained the molar volume using the sessile drop method.

depending on the alloy system. This shows the need for highly accurate experimental values.

### 3.3 Correlation between excess volume and excess Gibbs energy

Iida and Guthrie [23] presented the diagram showing the correlation between  $H^E$  and  $V^E$  for liquid binary alloys. They pointed out that negative  $V^E$  values have been observed for compound-forming alloy systems, and that positive  $V^E$  indicates repulsive interactions between different kinds of atoms. They also said that reliable and systematic data for the density of liquid binary alloys were scarce, and therefore it was difficult to make a detailed comparison between experiment and theory. We have proposed a diagram showing the correlation between  $G^E$  and  $V^E$  instead of between  $H^E$  and  $V^E$ , because equilibrium atomic arrangement in liquid binary alloys should be determined by both enthalpy and entropy terms. Figure 4 shows the correlation between  $G^E$  and  $V^E$  for various liquid binary alloys at a composition of 0.5 mole fraction of each alloy [16]. We note that there are two trends, cases 1 and 2 as shown in Fig. 4. The alloys in case 1 have a positive correlation between  $G^E$  and  $V^E$ . By contrast, the alloys in case 2 show a negative correlation between them. Case 1 is understandable from the classical principle stated by Iida and Guthrie. However, straightforward interpretation of case 2 has not been reached yet. In the next section, we introduce a model to understand the behavior of case 2 using the phase diagram and electronic structure.

### 3.4 Discussion of systems with positive $V^E$ and negative $G^E$

Pd-X [16] and Pt-X (where X is Fe, Co, Ni, or Cu) alloys [20] are typical case 2 systems. They have a common feature in their phase diagrams. Figure 5 is the Pd-Fe binary phase diagram [24] as an example. This diagram shows a wide solid solution under the liquid phase, and there are order-disorder

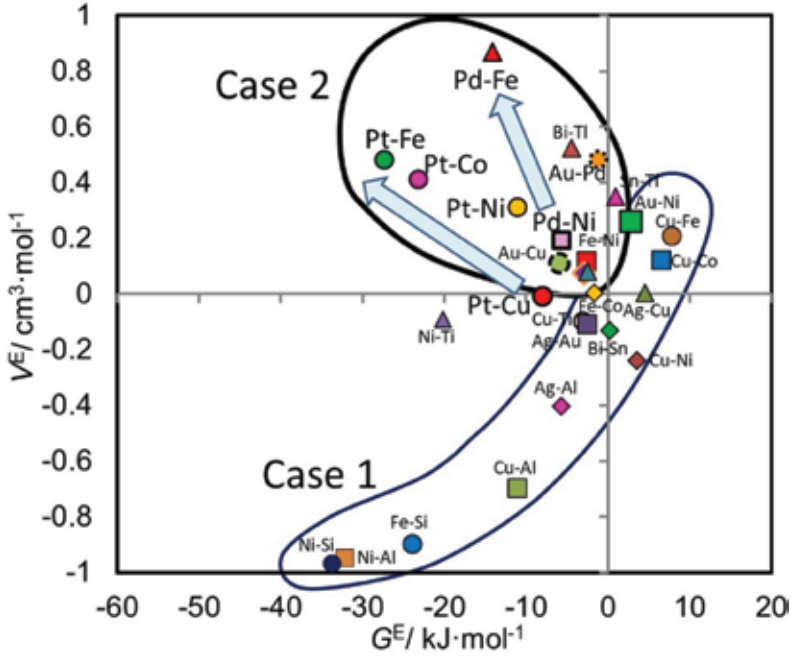


FIGURE 4 Correlation between excess volume and excess Gibbs energy for various binary melts at 0.5 mole fraction [16]. The data for the Pt-X systems (where X is Fe, Co, Ni, and Cu) are reported elsewhere [20].

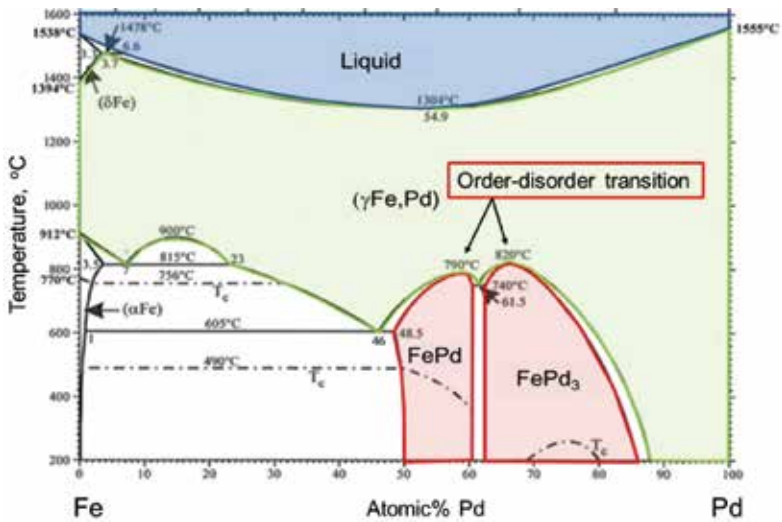


FIGURE 5 Pd-Fe binary phase diagram [24].

transitional compounds ( $\text{FePd}$  and  $\text{FePd}_3$ ) in the solid solution. Other Pd-X and Pt-X systems also have order-disorder transitions.

We should also point out that the  $V^E$  values of the Pd-X and Pt-X systems increase with the transition metal order in the periodic table (i.e., Fe, Co, Ni, and Cu) as shown by the arrows in Fig. 4. This implies that the electronic structure of the alloy systems is most probably related to case 2 behavior (positive  $V^E$  with negative  $G^E$ ).

Van Acker *et al.* [25] studied the photoemission of the electronic structure of Pd-Fe alloys using synchrotron radiation. They found that the binding energy of the Pd-4*d* state increased with Fe content, and the Fe minority-spin band (Fe-3*d*<sup>-</sup> state) gradually emptied with increasing Fe dilution. They concluded that covalent interaction existed between the Pd-4*d* and Fe-3*d* states, and they proposed an energy diagram indicating this covalent interaction. On the basis of their results, we propose a model explaining the negative correlation between  $V^E$  and  $G^E$  found in case 2. Figure 6 is our revision of the energy diagram proposed by van Acker *et al.* This figure shows that covalent interaction occurs between Pd-4*d* and Fe-3*d* states in the Pd-Fe alloys, and the remaining Fe-4*s* electron is shielded by this covalent interaction. Thus, the covalent orbital formation corresponds to the negative thermodynamic values ( $H^E < 0$  and  $G^E < 0$ ). This expands the orbital of the Fe-4*s* electron shielded by the covalent interaction, which corresponds to positive excess volume ( $V^E > 0$ ). This model is based on the photoemission study by van Acker *et al.* on solid alloys at room temperature. We plan to develop a metallic solution model based on a high-temperature photoemission study of liquid

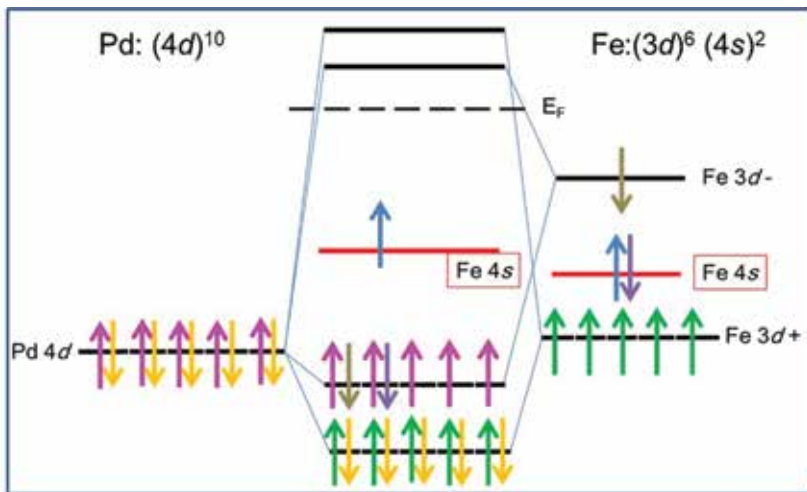


FIGURE 6  
Energy diagram indicating the covalent interaction between Fe 3*d* and Pd 4*d* states in Pd-Fe alloys.



alloys using synchrotron radiation combined with first-principle theory in the near future.

## 4 EXCESS HEAT CAPACITY

### 4.1 Laser modulation calorimetry

We developed non-contact laser modulation calorimetry in 2007. This function has been installed in PROSPECT, which enables heat capacity measurements via modulated laser irradiation on a levitated sample droplet. The true thermal conductivity of a sample droplet can be also measured with this technique under a static magnetic field, which effectively suppresses convection in the droplet [1,2,26]. Here, we present the heat capacity measurement and its excess function.

Figure 1(c) is the schematic of the laser modulation calorimetry, where the laser irradiates the top of a sample droplet with modulated power, and the temperature response is measured via radiation pyrometry from the bottom of the sample. It is necessary to keep the sample in an adiabatic condition during the measurement. The Biot number should be small enough to realize the adiabatic condition, which means the external heat transfer from the sample surface should be much lower than the internal heat conduction. The sample droplet levitated in PROSPECT has strong convections consisting of buoyancy convection, Marangoni convection, and magnetohydrodynamic convection. These convections greatly improve internal heat transfer, which should remain. For this reason, a small static magnetic field should be applied only to suppress sample oscillation and translational motion. We should note that a strong static magnetic field is necessary for measuring the thermal conductivity, which is not the case for measuring the heat capacity. Thus, selecting a static magnetic field is important for the laser modulation calorimetry. We obtained the phase shift between the modulated laser power and temperature response as a function of modulation frequency. The adiabatic condition is almost fulfilled around the modulation frequency with a phase shift of  $90^\circ$ . The laser power absorptivity should be determined before the calorimetry. We used the normal spectral emissivity at a laser wavelength of 940 nm as the laser power absorptivity [14].

### 4.2 Heat capacity and excess heat capacity of Fe-Ni melts

Figure 7 shows the variation of the molar heat capacity  $C_p$  with temperature for Fe-Ni melts of various compositions [14]. Our data for pure Fe and Ni are 44.0 and 40.8 J·mol<sup>-1</sup>·K<sup>-1</sup>, respectively, which agree with the values in the NIST-JANAF thermochemical tables [27] (46.024 and 38.911 J·mol<sup>-1</sup>·K<sup>-1</sup>, respectively) within the present expanded uncertainty (5–15%). Figure 7 reveals that  $C_p$  for all the alloys has no temperature dependence in the temperature ranges we measured. This is also supported by the NIST-JANAF thermochemical tables for pure Fe and Ni.

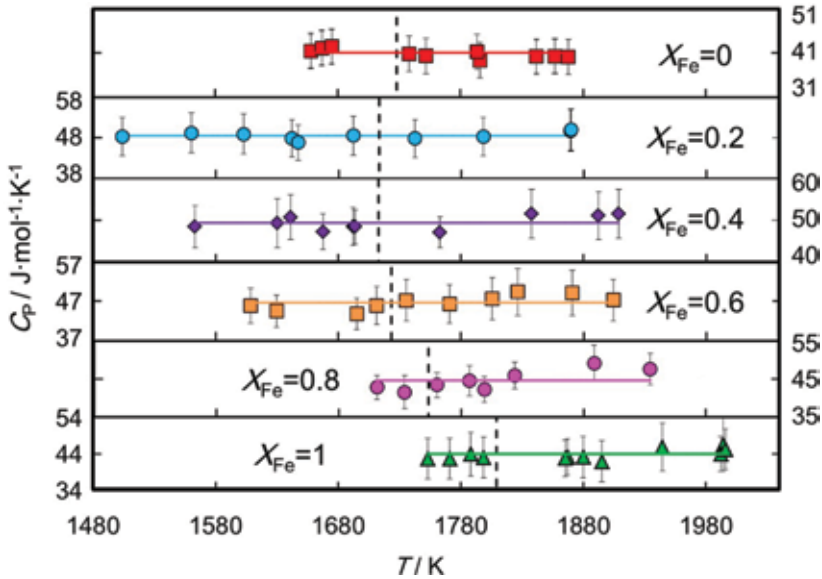


FIGURE 7 Variation of molar heat capacity  $C_p$  with temperature for various compositions of Fe-Ni melts [14].

Figure 8(a) shows the variation of the molar heat capacity  $C_p$  with composition for the Fe-Ni melts at temperatures from 1753 to 1869 K [14]. The experimental data reveal a positive deviation from those for an ideal solution, which are indicated by the dashed line over the entire composition range. This dashed line is the Neumann-Kopp rule [23], which has been used to estimate the heat capacity of liquid alloys by proportionally adding the heat capacities of the constituent elements. The deviation of the measured values from an ideal solution is the excess heat capacity  $C_p^E$ , whose composition dependence is shown in Fig. 8(b). Thus,  $C_p^E$  is positive over the entire composition range. These results provide important guidelines as explained next.

### 4.3 Discussion on excess heat capacity

In 1966, Lupis and Elliott stated that an increase in temperature tends to bring a system closer to ideality (the Lupis-Elliott rule) [29,30]. Kaptay [31] reformulated this statement in 2012 as, “Real solid, liquid and gaseous solutions (and pure gases) gradually approach the state of an ideal solution (perfect gas) as temperature increases at any fixed pressure and composition.” Kaptay stated that the necessary and sufficient conditions to obey the Lupis-Elliott rule are: 1) the mixing heat and excess mixing entropy have equal signs, and 2) the mixing heat and excess heat capacity of mixing have opposite signs for the same solution.

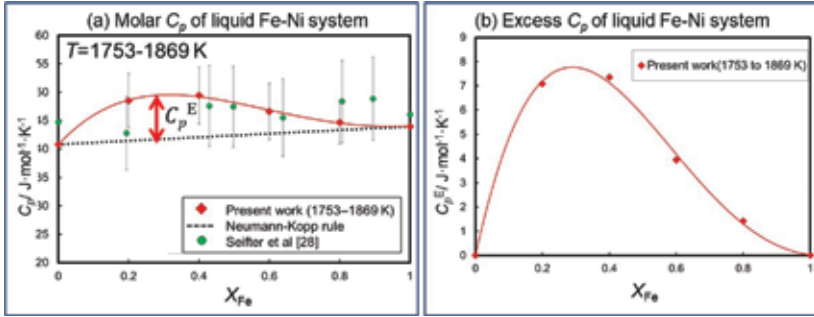


FIGURE 8

Variation of (a) molar heat capacity  $C_p$  and (b) excess heat capacity  $C_p^E$  with composition for Fe-Ni melts at temperatures from 1753 to 1869 K [14]. The present data show good agreement with previous results reported by Seifert et al. (pulse-heating technique) [28] within experimental uncertainty.

Our results in Fig. 8 show  $C_p^E > 0$ ; therefore, our model predicts  $H^E < 0$  and  $S^E < 0$  for the Fe-Ni melts. Predel and Mohs [32] and Batalin et al. [33] reported negative  $H^E$  values at 1873 K for the entire composition range of the Fe-Ni melts. Assuming that  $C_p^E$  has no temperature dependence, the following equation is obtained:

$$H^E(T) = H^E(T_{\text{ref}}) + C_p^E \int_{T_{\text{ref}}}^T dT. \quad (7)$$

The temperature dependence of  $H^E$  is evaluated with the  $C_p^E$  values obtained in this study using Eq. (7) and plotted in Fig. 9(a). Here,  $T_{\text{ref}}$  is 1873 K, and  $H^E(T_{\text{ref}})$  is the average of the values reported by Predel and Mohs [32] and by Batalin et al. [33]. Thus,  $H^E$  is negative with positive  $C_p^E$ , and  $H^E$  approaches its ideal solution with increasing temperature, which agrees with the Lupis-Elliott rule [29,30] and the Kaptay statement [31].

The value of  $S^E$  was calculated from the relation  $S^E = (H^E - G^E)/T$ . The  $G^E$  value of the Fe-Ni melts was obtained by averaging the values reported by Zellar et al. [34], Belton and Fruehan [35], Speiser et al. [36], Maruyama and Ban-ya [37], and Rammensee and Franser [38]. Assuming that  $C_p^E$  has no temperature dependence, the following equation is obtained:

$$S^E(T) = S^E(T_{\text{ref}}) + C_p^E \int_{T_{\text{ref}}}^T \frac{1}{T} dT. \quad (8)$$

Figure 9(b) shows the temperature dependence of  $S^E$  determined with the  $C_p^E$  values obtained in this study using Eq. (8). Thus,  $S^E$  is negative with positive  $C_p^E$ , and again  $S^E$  approaches an ideal solution with increasing temperature. This also agrees with the Lupis-Elliott rule [29,30] and the Kaptay statement [31].

We note that Eqs. (7) and (8) are only valid in a limited temperature range, because they are derived assuming that  $C_p^E$  is independent of temperature. In

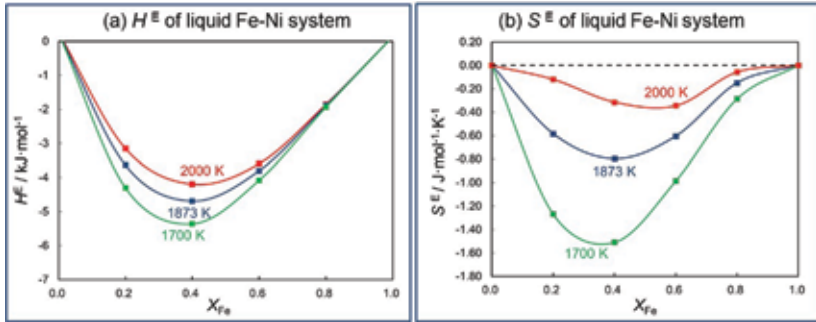


FIGURE 9 Temperature dependence of (a)  $H^E$  and (b)  $S^E$  determined with the  $C_p^E$  values obtained in this study.

addition, the excess Gibbs energy  $G^E$  does not approach an ideal solution with increasing temperature even in the limited range under this assumption. Considering that all the excess properties should approach zero as the temperature approaches infinity,  $C_p^E$  should approach zero as temperature increases. Here,  $C_p^E$  is treated as a constant for each alloy composition; however, it should have a very small negative temperature dependence to meet the Lupis-Elliott rule.

## 5 SUMMARY

We developed PROSPECT, which contributes useful data to high-temperature material science. Precise measurement of thermophysical properties provides accurate excess functions, which represent non-ideality of solutions. We have used excess functions to discuss a solution model in terms of electronic structure and thermodynamics.

Pd-X and Pt-X systems have positive  $V^E$  with negative  $G^E$ . A common feature of these systems is the order-disorder transition in each of their phase diagrams. We discussed the correlation between  $V^E$  and  $G^E$  for the Pd-Fe alloy melts in terms of the electronic structure of the alloys. Further photoemission study on high-temperature liquid alloys is necessary to understand this behavior.

The  $C_p^E$  values of Fe-Ni melts are positive over our whole composition range and a wide temperature range. We determined the temperature dependences of  $H^E$  and  $S^E$  for Fe-Ni melts from  $C_p^E$ . The Lupis-Elliott rule was satisfied for  $H^E$  and  $S^E$  via  $C_p^E$ . From the Lupis-Elliott rule, we suggest that  $C_p^E$  should have a slightly negative temperature dependence in Fe-Ni melts.

## ACKNOWLEDGEMENTS

We are grateful to Professors Taketoshi Hibiya (Keio University), Takao Tsukada (Tohoku University), Masahito Watanabe (Gakushuin University),

Shumpei Ozawa (Chiba Institute of Technology), and Hidekazu Kobatake (Hirosaki University), as well as all members of Fukuyama Laboratory for performing measurements to develop PROSPECT. H. F. greatly appreciates fruitful discussion with Prof. Ivan Egry. This work was supported by the Japan Society for the Promotion of Science (KAKENHI Grant Numbers 26249113 and 18J11474).

## REFERENCES

- [1] Fukuyama, H., Kobatake, H., Takahashi, K., Minato, I., Tsukada, T., Awaji, S., *Meas. Sci. Technol.*, **18** (2007) 2059. DOI: 10.1088/0957-0233/18/7/036.
- [2] Kobatake, H., Fukuyama, H., Tsukada, T., Awaji, S., *Meas. Sci. Technol.*, **21** (2010), 025901. DOI: 10.1088/0957-0233/21/2/025901.
- [3] Kobatake, H., Khosroabadi, H., Fukuyama, H., *Meas. Sci. Technol.*, **22** (2011), 015102. DOI: 10.1088/0957-0233/22/1/015102.
- [4] Sugie, K., Kobatake, H., Fukuyama, H., Baba, Y., Sugioka, K., Tsukada, T., *Tetsu-to-Hagane*, **96** (2010), 673. DOI: 10.2355/tetsutohagane.96.673.
- [5] Sugie, K., Kobatake, H., Uchikoshi, M., Isshiki, M., Sugioka, K., Tsukada, T., Fukuyama, H., *Jpn. J. Appl. Phys.*, **50** (2011), 11RD04. DOI: 10.7567/JJAP.50.11RD04.
- [6] Kobatake, H., Khosroabadi, H., Fukuyama, H., *Metall. Mater. Trans. A*, **43A** (2012), 2466. DOI: 10.1007/s11661-012-1101-0.
- [7] Morohoshi, K., Uchikoshi, M., Isshiki, M., Fukuyama, H., *ISIJ Int.*, **51** (2011), 1580. DOI: 10.2355/isijinternational.51.1580.
- [8] Fukuyama, H., Morohoshi, K., Uchikoshi, M., Isshiki, M., *ISIJ Int.*, **54** (2014), 2109. DOI: 10.2355/isijinternational.54.2109.
- [9] Baba, Y., Inoue, T., Sugioka, K., Kobatake, H., Fukuyama, H., Kubo, M., Tsukada, T., *Meas. Sci. Technol.*, **23** (2012), 045103. DOI: 10.1088/0957-0233/23/4/045103.
- [10] Kurosawa, R., Inoue, T., Baba, Y., Sugioka, K., Kubo, M., Tsukada, T., Fukuyama, H., *Meas. Sci. Technol.* **24** (2013), 015603. DOI: 10.1088/0957-0233/24/1/015603.
- [11] Watanabe, M., Takano, J., Adachi, M., Uchikoshi, M., Fukuyama, H., *J. Chem. Thermodynamics*, **121** (2018), 145. DOI: 10.1016/j.jct.2018.02.004.
- [12] Brillo, J., Wessing, J., Kobatake, H., Fukuyama, H., *J. Mol. Liquids*, **290** (2019), 111226. DOI: 10.1016/j.molliq.2019.111226.
- [13] Watanabe, M., Adachi, M., Fukuyama, H., *J. Mater. Sci.*, **51** (2016), 3303. DOI: 10.1007/s10853-015-9644-2.
- [14] Watanabe, M., Adachi, M., Fukuyama, H., *J. Mater. Sci.*, **52** (2017), 9850. DOI: 10.1007/s10853-017-1122-6.
- [15] Adachi, M., Sato, A., Hamaya, S., Ohtsuka, M., Fukuyama, H., *SN Appl. Sci.*, (2019) 1:18, DOI: 10.1007/s42452-018-0023-x.
- [16] Watanabe, M., Adachi, M., Fukuyama, H., *J. Chem. Thermodynamics*, **130** (2019), 9. DOI: 10.1016/j.jct.2018.09.037.
- [17] Mizuno, A., Kawauchi, H., Tanno, M., Murai, K., Kobatake, H., Fukuyama, H., et al., *ISIJ Int.*, **54** (2014), 2120. DOI: 10.2355/isijinternational.54.2120.
- [18] Sugioka, K., Inoue, T., Kitahara, T., Kurosawa, R., Kubo, M., Tsukada, T., et al., *Metall. Mater. Trans. B*, **45B** (2014), 1439. DOI: 10.1007/s11663-014-0052-9.
- [19] Watanabe, M., Adachi, M., Fukuyama, H., *J. Mater. Sci.*, **54** (2019), 4306. DOI: 10.1007/s10853-018-3098-2.
- [20] Watanabe, M., Adachi, M., Uchikoshi, M., Fukuyama, H., submitted to *J. Mol. Liquids*.
- [21] Fukuyama, H., Higashi, H., Yamano, H., *Nuclear Technology*, 205 (2019), 1154. DOI: 10.1080/00295450.2019.1578572.
- [22] Ukhov, V. F., Dubinin, E. L., Esin, O. A., *Zhurnal Fizicheskoi Khimii* (= *Russ. J. Phys. Chem.*), **42** (1968), 1391.
- [23] Iida, T., Guthrie, R. I. L., *The physical properties of liquid metals*. Clarendon Press, Oxford, 1988.

- [24] Okamoto, H., *Phase Diagrams for Binary Alloys*, ASM International, Materials Park, OH, 2000, pp. 370.
- [25] van Acker, J. F., Weijs, P. J. W., Fuggle, J. C., Horn, K., Haak, H., Buschow, K. H. J., *Phys. Rev. B*, **43** (1991), 8903. DOI:10.1103/PhysRevB.43.8903.
- [26] Tsukada, T., Fukuyama, H., Kobatake, H., *Int. J. Heat Mass Transfer*, **50** (2007), 3054. DOI: 10.1016/j.ijheatmasstransfer.2006.12.026.
- [27] *NIST-JANAF Thermochemical tables 4th Ed.*, J. Phys. Chem. Ref. Monograph, No.9, 1998.
- [28] Seifert, A., Pottlacher, G., Jäger, H., Groboth, G., Kaschnitz, E., *Ber Bunsenges Phys Chem.*, **102** (1998), 1266. DOI: 10.1002/bbpc.19981020934.
- [29] Lupis, C. H. P., Elliott, J. F., *Trans. Met. Soc. AIME*, **236** (1966), 130.
- [30] Lupis, C. H. P., Elliott, J. F., *Acta Metall.*, **15** (1967), 265. DOI: 10.1016/0001-6160(67)90202-7.
- [31] Kaptay, G., *Metall. Mater. Trans. A*, **43A** (2012), 531. DOI: 10.1007/s11661-011-0902-x.
- [32] Predel, B., Mohs, R., *Arch Eisenhüttenwes*, **41** (1970), 143. DOI: 10.1002/srin.197001581.
- [33] Batalin, G. I., Minenko, N. N., Sudavtsova, V. S., *Russ Metall.*, **5** (1974), 99.
- [34] Zellar, G. R., Payne, S. L., Morris, J. P., Kipp, R. L., *Trans. Metall. Soc. AIME.*, **215** (1989), 181.
- [35] Belton, G. R., Fruehan, R. J., *J. Phys. Chem.*, **71** (1967), 1403. DOI: 10.1021/j100864a034.
- [36] Speiser, R., Jacobs, A. J., Spretnak, J. W., *Trans. Metall. Soc. AIME*, **215** (1959), 185.
- [37] Maruyama, N., Ban-ya, S., *J. Jpn. I. Met.*, **42** (1978), 992. DOI: 10.2320/jinstmet1952.42.10\_992.
- [38] Rammensee, W., Franser, D. G., *Phys. Chem.*, **85** (1981), 588 DOI: 10.1002/bbpc.19810850713.